Proceedings of the 21st ICSMGE, Vienna, Austria, 14 – 19 June 2026. Pistrol, Adam & Schweiger (eds.)
Published by: ÖGG, Austrian Society for Geomechanics, Salzburg, Austria, ISBN 978-3-9503898-4-5
https://doi.org/10.53243/ICSMGE2026-177

Parametric study of cylindrical shafts behavior

Elena-Mihaela Stan, Horațiu Popa
Geotechnical Engineering Department, Technical University of Civil Engineering, Bucharest, Romania,
elena-mihaela.stan@phd.utcb.ro

ABSTRACT: The behavior of the cylindrical shafts is not completely understood and there are few theoretical calculation methods. This paper presents the results of a numerical parametric study of the cylindrical shafts behavior conducted using the finite element method in 3D and axisymmetric conditions. For this study, the cylindrical shafts radius, the length and the thickness of the diaphragm wall and the excavation deep have been varied. To analyze the influence of the surrounding soil, two types of soil have been used, cohesive and cohesionless. The results show the minimum necessary length of the diaphragm wall in relation to the excavation depth, the relation between the maximum lateral displacements of the wall and the cylindrical shaft radius, the earth pressure distribution for the two types of soil and its comparison with theoretical methods known in literature.

KEYWORDS: numerical modelling, cylindrical shafts, deep excavation, earth pressure distribution, lateral displacements.

1 INTRODUCTION

Limited information is available on the behavior and structural analysis of cylindrical shafts, primarily due to their specific shape and functional roles such as pumping stations, TBM launch shafts, tunnel access with staircases or elevators, ventilation systems or underground parking structures.

Using classical earth pressure theories for the calculation of cylindrical shafts can lead to an overdesigned structure because the arching effect is neglected.

The first studies regarding earth pressure acting on cylindrical shafts were performed by Westergaard (1940) and Terzaghi (1943). They have shown that the hoop and radial stresses decrease radially as they approach the cylindrical shafts. This phenomenon is known as the arching effect. At the same time, the radial stress increases with depth until it reaches a constant value. According to Prater (1977), the lateral earth pressure increases with depth to a peak value, then decreases until it reaches a zero value. Also, a conical failure surface is proposed. Several experimental studies (Tobar & Meguid 2009) have shown that the lateral earth pressure distribution is consistent with Terzaghi's (1943) theoretical model.

A numerical parametric study was performed in order to analyze the behavior of cylindrical shafts using the finite difference method (Tangjarusritaratorn et al. 2022). The lateral earth pressure distribution did not correspond perfectly with that of the known analytical theories. The lateral displacements of the retaining wall gradually increase with depth, attaining a maximum value 10-20 meters above the final excavation level.

Based on in-situ measurements, New & Bowers (1994) proposed an equation to approximate the vertical displacements of the soil. Later, Schwamb & Soga (2015) compared the ground vertical displacements obtained using this equation with field measurements. The measured vertical displacements were smaller than those calculated using the equation. This discrepancy may be due to the fact that the proposed equation does not account for the shaft diameter and also relies on an empirically chosen constant.

Le et al. (2019) conducted a physical model study of cylindrical shafts and measured the lateral displacements of the surrounding soil. They proposed an equation to calculate these lateral displacements. However, the equation does not account for the shaft diameter. The maximum lateral displacement occurs at a depth of 0.6 to 0.8 times the final excavation depth.

The finite element method (FEM) is widely used in geotechnical engineering because it allows for soil-structure interaction modelling. The finite element method in 2D axisymmetric or 3D conditions can be employed to model the cylindrical shafts. This paper presents the results of a parametric study conducted using the 3D finite element method to analyze the behavior of cylindrical shafts. Additionally, the 2D axisymmetric finite element method has been used to compare the two methods.

2 NUMERICAL MODELLING

To analyze the cylindrical shafts behavior in terms of lateral earth pressure and retaining wall lateral displacements, the 3D finite element method was employed. The numerical modelling has been carried out using the Plaxis 3D design software.

A parametric study was conducted in which the excavation depth (H), diaphragm wall length (L) and cylindrical shaft radius (r) were varied. The values of these parameters are shown in Table 1 (the radius, excavation depth and diaphragm wall length were varied in increments of 1 or 5 meters within the given interval).

Table 1. The parameters included in the parametric study.

Soil type	Radius (r) [m]	Excavation depth (H) [m]	Diaphragm wall length (L) [m]	Number of models
cohesive (C)	10 - 560	10 - 50	11 - 100	678
cohesionless (NC)	10 - 1000			714
		Total number of models		1392

Two types of soil have been used for this parametric study: cohesive (C) and cohesionless (NC), both modeled using the Hardening Soil Model. The parameters for the two soil types are presented in Table 2.

Table 2. Soil parameters used in the numerical analyses

Soil type	γ [kN/m^3]	E_{50}^{ref} [kPa]	E_{oed}^{ref} [kPa]	E_{ur}^{ref} [kPa]	c' [kPa]	ϕ' [°]	R_{inter} [-]
NC	19.5	25000	25000	75000	5	30	0.67
C	19.5	15000	15000	45000	40	15	0.67

Where:

- γ – unit weight
- E_{50}^{ref} – secant stiffness in standard drained triaxial test
- E_{oed}^{ref} – tangent stiffness for primary oedometer loading
- E_{ur}^{ref} – unloading/reloading stiffness
- c' – effective cohesion
- ϕ' – effective angle of internal friction
- R_{inter} – strength reduction factor.

The diaphragm wall is modelled as plate and the capping beam as a beam element. The linear elastic constitutive model has been used for each. For both, the concrete modulus of elasticity is $3.1 \cdot 10^7$ kPa, the unit weight is 25 kN/m^3 and Poisson's ration

is 0.2. The diaphragm wall thickness is 0.45 m, and the height and width of the capping beam are 0.45 m and 0.60 m, respectively.

The numerical model dimensions are selected based on the excavation depth, with the model being extended to five times the excavation depth upstream of the diaphragm wall and three times below the excavation.

3 RESULTS AND DISCUSSIONS

3.1 *The lateral earth pressure*

Figure 1and Figure 2 show the lateral earth pressure diagrams for a cylindrical shaft with an excavation depth of 10m and a diaphragm wall length of 20m. The shaft radius (r) varies between 10 and 1000m in the case of cohesionless soil (Figure 1), and between 10 and 560m in the case of cohesive soil (Figure 2). Also, the active and at-rest earth pressures calculated according to Rankine's theory were plotted for analysis. The at-rest earth pressure coefficient was calculated using Jaky's empirical relation (Equation (1)) for both types of soil, this relation also being used by the Plaxis 3D software.

$$k_0 = 1 - \sin(\phi) \quad (1)$$

Generally, for all geometric characteristics and soil types considered in this study, the lateral earth pressure diagrams did not match those obtained using the numerical methods described in the previous chapter. The results of this study are consistent with those reported by Tangjarusritaratorn et al. (2022), who used the finite difference method.

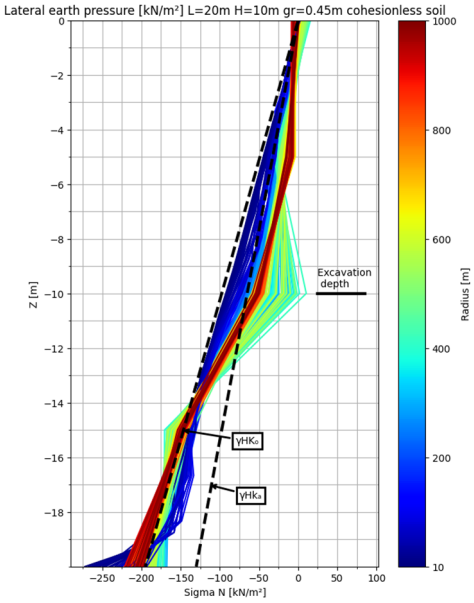

Figure 1. The lateral earth pressure diagrams for a cylindrical shaft with H=10m, L=20m, r between 10 and 1000m, cohesionless soil

In the case of cohesionless soil and shaft radii ranging from 10 to 100m, the lateral earth pressure falls between the active and at-rest earth pressure values. The lateral earth pressure increases approximately linearly with depth, and its values are closer to those of the at-rest earth pressure. For larger radii, the lateral earth pressure diagrams no longer increase linearly with depth, and at the excavation depth, their values are lower than those of the active earth pressure.

In the case of cohesive soil, the lateral earth pressure values are greater than those observed for cohesionless soil. However, the lateral earth pressure increases approximately linearly with depth, and its variation with respect to shaft radius is smaller than in the case of cohesionless soil. Moreover, the lateral earth pressure values do not decrease below the active earth pressure values.

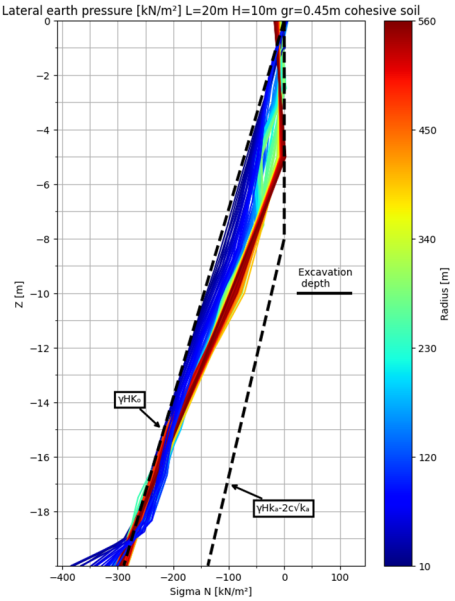

Figure 2. The lateral earth pressure diagrams for a cylindrical shaft with H=10m, L=20m, r between 10 and 560m, cohesive soil

3.2 *The lateral displacements of the retaining structure*

Figure 3 shows the lateral displacement diagrams of the diaphragm wall for a cylindrical shaft with an excavation depth of 10m and a diaphragm wall length of 20m, modeled in cohesive soil. To analyze the arching effect, the shaft radius (r) varies between 10 and 560m. Additionally, the lateral displacement diagram for an excavation with the same characteristics, but calculated using plane strain conditions, is plotted.

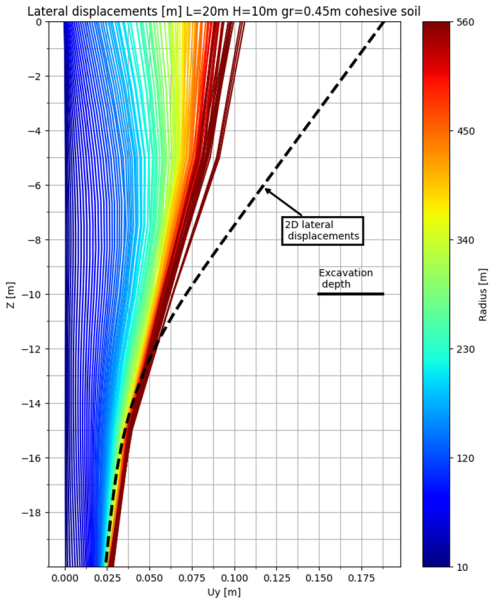

Figure 3. The lateral displacements of the diaphragm wall for a cylindrical shaft with H=10m, L=20m, r between 10 and 560m, cohesive soil

Due to the arching effect, the maximum lateral displacement of the diaphragm wall occurs above the excavation depth. For radii greater than 300m, this behavior changes, and the maximum lateral displacement occurs at the top of the wall. This behavior is specific to plane strain conditions, indicating that the arching

effect is diminished. However, even for a large radius of 560m, the maximum lateral displacement of the diaphragm wall remains smaller than that obtained from the plane strain analysis.

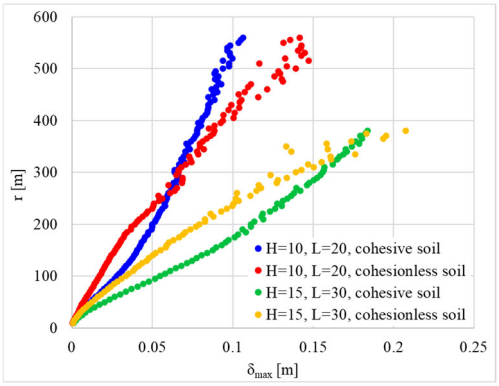

Figure 4. Variation of the maximum lateral displacement of the diaphragm wall with shaft radius and soil type

The maximum lateral displacement of the diaphragm wall increases with increasing shaft radius and excavation depth. For each combination of excavation depth and soil type, its variation with radius exhibits a consistent trend.

Up to a certain shaft radius, the maximum lateral displacements of the diaphragm wall are greater when the excavation is modeled in cohesive soil compared to cohesionless soil. Beyond this radius, the maximum lateral displacements become larger for excavation in cohesionless soil than for those in cohesive soil. For the two given excavation depths (Figure 4), this transition occurs for:

$$r = (21 \div 26)H \qquad (2)$$

3.3 *The compressive hoop stress*

Figure 5 shows the compressive hoop stress diagrams for a cylindrical shaft with the excavation depth of 10m, the length of the diaphragm wall of 20m, shaft radii between 10 and 560m, modeled in cohesive soil.

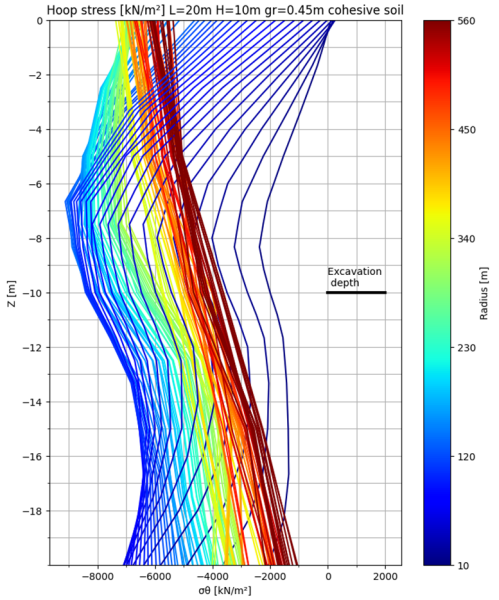

Figure 5. The compressive hoop stress for a cylindrical shaft with H=10m, L=20m, r between 10 and 560m, cohesive soil

The compressive hoop stress increases with shaft radius. Similar to the lateral displacement of the diaphragm wall, its distribution changes for large radii. In such cases, the maximum compressive hoop stress no longer occurs above the final excavation depth, but rather at the top of the diaphragm wall. This behavior indicates a reduction in the arching effect. A similar trend is observed for cylindrical shafts modeled in cohesionless soil.

Figure 6 shows the ratio between the depth at which the maximum compressive hoop stress occurs and the depth at which the maximum lateral displacement of the diaphragm wall occurs, both normalized by the excavation depth.

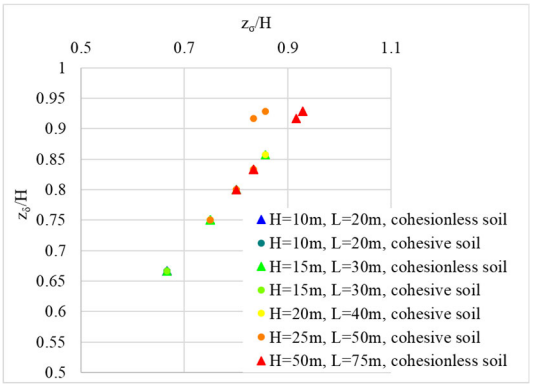

Figure 6. The ratio between the normalized depth of the maximum compressive hoop stress (z_σ/H) and the normalized depth of the wall's maximum lateral displacement (z_δ/H), relative to the excavation depth

The maximum compressive hoop stress and the maximum lateral displacement of the diaphragm wall occur at the same depth.

3.4 *The minimum length of the retaining wall*

For each type of soil, numerical models of cylindrical shafts have been conducted, in which the length of the diaphragm wall was varied from the excavation depth plus 1m to twice the excavation depth.

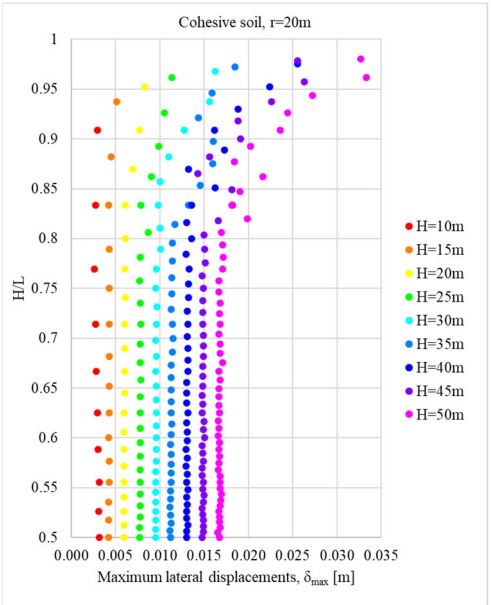

Figure 7. Variation of the maximum lateral displacement (δ_{max}) with the excavation depth normalized by the diaphragm wall length (H/L)

Figure 7 shows the variation of the maximum lateral displacement (δ_{max}) with the excavation depth (H), normalized by the diaphragm wall length (L), for a cylindrical shaft with a radius of 20m in cohesive soil. A decrease in the variation of the maximum displacement of the retaining wall is observed, regardless of the excavation depth considered, starting from an H/L ratio of 0.80.

A similar approach was applied to the hoop stress in the retaining wall. Thus, Figure 8 shows the variation of the maximum hoop stress (σ_{max}) with the excavation depth (H), normalized by the diaphragm wall length (L), for the same cylindrical shafts as those described above. Starting from an H/L ratio of about 0.83, the variation in maximum hoop stress becomes insignificant.

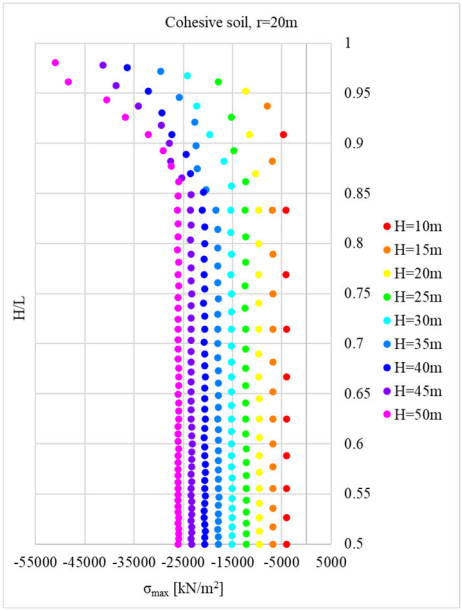

Figure 8. Variation of the maximum hoop stress (σ_{max}) with the excavation depth normalized by the diaphragm wall length (H/L)

Figure 9 shows the bending moment diagrams for a cylindrical shaft with an excavation depth of 20m and a shaft radius of 20m, modeled in cohesive and cohesionless soil. The diaphragm wall length varies from the excavation depth plus 1m to twice the excavation depth. Despite the large excavation depth, the maximum bending moment remains low for all lengths, with values below 100kNm/m.

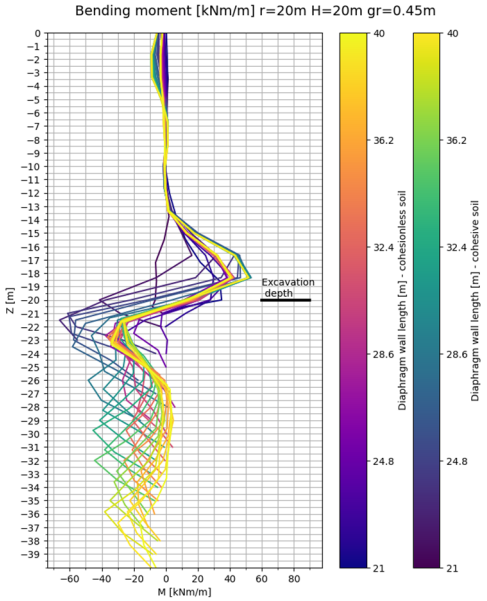

Figure 9. Bending moment diagrams [kNm/m] for a cylindrical shaft with r=20m and H=20m, in cohesive and cohesionless soils, with varying diaphragm wall lengths

Considering the maximum lateral displacement, the maximum hoop stress in the retaining wall and the bending moment, a minimum length corresponding to an H/L ratio of 0.80 is recommended.

Table 3. Differences between the maximum lateral displacements in cohesive and cohesionless soils

H/L=0.8	H [m]	10	15	20	25	30
δ_{max} [mm]	cohesive	2.60	4.30	6.10	7.80	10.1
	cohesionless	1.70	2.80	4.00	5.00	6.20
$\Delta\delta_{max}$ [%]		52.8	52	53.3	56.2	63.7

For cylindrical shafts with the same radius, excavation depths and retaining wall lengths chosen based on an H/L ratio of 0.80, the maximum lateral displacements of the retaining system, when the cylindrical shaft is modeled in cohesive soil, are 52-64% greater than those modeled in cohesionless soil.

4 CONCLUSIONS

To analyze the behavior of cylindrical shafts, a parametric study was carried out in which various shaft characteristics were varied: excavation depth, diaphragm wall length, shaft radius and soil type (cohesive and cohesionless). The numerical modeling was conducted using the finite element method under 3D conditions.

The results show the lateral earth pressure diagrams for different shaft radius values and their comparison with the active and at-rest earth pressure diagrams. For shaft radii smaller than 100m, the lateral earth pressure values are close to the at-rest earth pressure and increase approximately linearly with depth. For larger radii, the variation of lateral earth pressure with depth differs depending on the soil type.

The lateral displacement diagrams show that the maximum lateral displacement occurs above the excavation depth due to the arching effect. For larger shaft radii, the maximum lateral displacement occurs at the top of the wall, indicating that the arching effect is diminished.

The maximum lateral displacement and compressive hoop stress occur at the same depth and vary with shaft radius and excavation depth.

Based on the maximum lateral displacement and maximum hoop stress, this study proposes a minimum diaphragm wall length, determined as a function of excavation depth.

5 REFERENCES

Le, B.T., Goodey, R.J., Divall, S., 2019. Subsurface ground movements due to circular shaft construction. *Soils and Foundations,* 59, 1160-1171

New, B.M., Bowers, K.H., 1994. Ground movement model validation at the Heathrow Express trial tunnel. *Tunnelling '94,* 301-329.

Prater, E.G., 1977. An examination of some theories of earth pressure on shaft linings. *Canadian Geotechnical Journal,* 14 (1), 91-106.

Schwamb, T., Soga, K., 2015. Numerical modelling of a deep circular excavation at Abbey Mills in London. *Geotechnique,* 65 (7), 604-619.

Tangjarusritaratorn, T., Miyazaki, Y., Sawamura, Y., Kishida, K., Kimura, M., 2022. Numerical investigation on arching effect surrounding deep cylindrical shaft during excavation process. *Underground Space,* 7, 944-965.

Terzaghi, K. 1943. Theoretical Soil Mechanics. New York: John Wiley and Sons.

Tobar, T., Meguid, M., 2009. Distribution of active earth pressure on vertical shafts. In: GeoHalifax2009 Organizing Committee, *62nd Canadian Geotechnical Conference & 10th Joint CGS/IAH-CNC Grounwater Conference.* Halifax, Nova Scotia, 20-23 september 2009.

Westergaard, H.M., 1940. Plastic state of stress around a deep well. *Journal of the Boston Society of Civil Engineers*, 27 (1), 387-391.